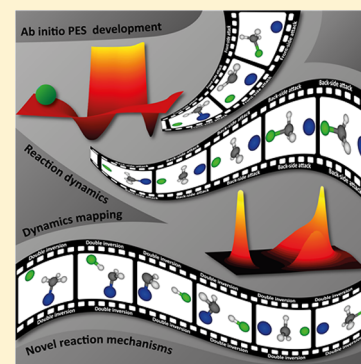


Dynamics and Novel Mechanisms of S_N2 Reactions on ab Initio Analytical Potential Energy Surfaces

István Szabó^a and Gábor Czakó^{*b}

Department of Physical Chemistry and Materials Science, Institute of Chemistry, University of Szeged, Rerrich Béla tér 1, Szeged H-6720, Hungary

ABSTRACT: We describe a novel theoretical approach to the bimolecular nucleophilic substitution (S_N2) reactions that is based on analytical potential energy surfaces (PESs) obtained by fitting a few tens of thousands high-level ab initio energy points. These PESs allow computing millions of quasi-classical trajectories thereby providing unprecedented statistical accuracy for S_N2 reactions, as well as performing high-dimensional quantum dynamics computations. We developed full-dimensional ab initio PESs for the $F^- + CH_3Y$ [$Y = F, Cl, I$] systems, which describe the direct and indirect, complex-forming Walden-inversion, the frontside attack, and the new double-inversion pathways as well as the proton-transfer channels. Reaction dynamics simulations on the new PESs revealed (a) a novel double-inversion S_N2 mechanism, (b) frontside complex formation, (c) the dynamics of proton transfer, (d) vibrational and rotational mode specificity, (e) mode-specific product vibrational distributions, (f) agreement between classical and quantum dynamics, (g) good agreement with measured scattering angle and product internal energy distributions, and (h) significant leaving group effect in accord with experiments.



I. INTRODUCTION

Understanding the atomic-level dynamics and mechanisms of chemical reactions is one of the fundamental goals of chemistry. Nearly 90 years after the birth of quantum mechanics we can perform accurate dynamical simulations for polyatomic chemical reactions by applying the laws of physics to the chemical systems using the tools of mathematics and informatics. Of course, the reaction dynamics computations still require several approximations. As shown in Figure 1, the Born–Oppenheimer approximation¹ separates the motion of the electrons from that of the much heavier nuclei. Then, first, the Schrödinger equation of the electrons is solved numerically employing one of the different electronic structure methods, such as Hartree–Fock,² Møller–Plesset perturbation theory,³ coupled cluster,⁴ density functional theories,⁵ etc. The electronic structure computations provide the potential energies, $E(\mathbf{R})$, electronic energy plus nuclear repulsion, at given fixed nuclear configurations (\mathbf{R}). Then, as the second step, one must describe the motion of the nuclei using either classical or quantum mechanical approaches. The latter is more rigorous but can only be applied to few-atom systems. Fortunately, the motion of the heavy nuclei can usually be well-described classically; thus, the former approach, especially its quasi-classical variant, which incorporates quantum effects into the initial conditions, is widely and successfully applied to study the dynamics of polyatomic chemical reactions. In both the classical and quantum cases one needs $E(\mathbf{R})$, because the quantum Hamiltonian is the sum of the nuclear kinetic energy and the potential energy, $E(\mathbf{R})$, operators, and in the classical case the forces are obtained from the gradients of $E(\mathbf{R})$ as seen in Figure 1. In the case of classical dynamics a popular approach is called direct dynamics, where the potential energies and

gradients are computed on-the-fly whenever needed during a reaction dynamics simulations. Since a quantitative dynamics study requires billions of gradients, direct dynamics is very time-consuming even if a low level of electronic structure theory is applied. Another approach develops an analytical representation of $E(\mathbf{R})$, thereby allowing efficient dynamical computations. An analytical potential energy surface (PES) can be developed by fitting few tens of thousands ab initio energy points; thus, one can afford using much higher level of electronic structure theory compared to the corresponding direct dynamics studies. We and others have successfully applied this analytic ab initio PES-based approach to the atom (F, O, Cl, Br) plus methane (CH_4, CHD_3 , etc.) hydrogen-abstraction reactions in the past nearly 10 years.^{6–10} However, for bimolecular nucleophilic substitution (S_N2) reactions traditionally the direct dynamics approach was used.^{11–15} Therefore, approximately five years ago we initialized a research program applying the above-described analytic PES-based approach to S_N2 reactions. We developed the first chemically accurate analytical PESs for S_N2 reactions,^{16–19} which made possible computing millions of trajectories, revealing a new S_N2 retention mechanism,¹⁷ performing quantum dynamics computations,²⁰ etc. In this article we are about to summarize our S_N2 story briefly describing the methodological details and featuring our recent results.

The story of S_N2 reactions began more than 100 years ago with the stereoselective conversions of optically active compounds performed by Paul Walden in 1896.²¹ Then, it

Received: August 15, 2017

Revised: September 16, 2017

Published: October 6, 2017



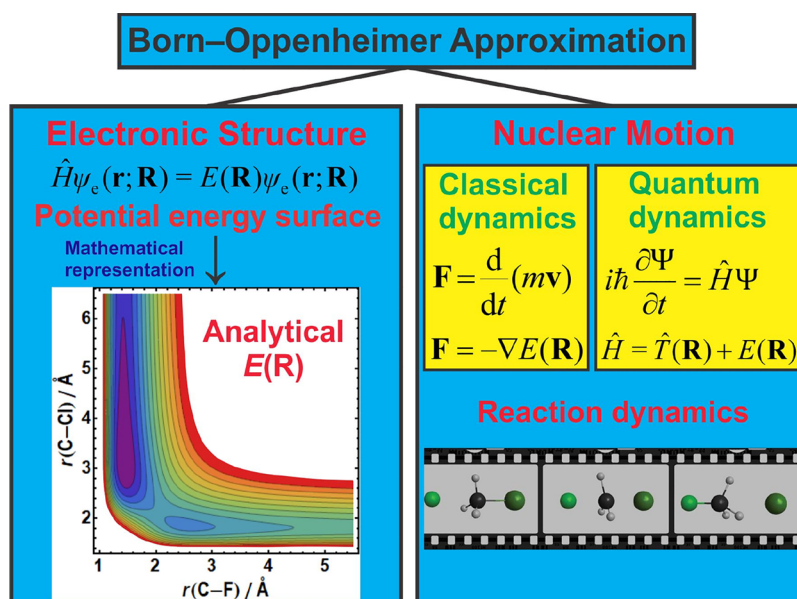
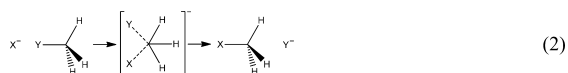


Figure 1. Graphical overview of our theoretical approach for studying the dynamics of S_N2 reactions.

took a few decades to explain the atomic-level mechanisms of these stereoselective processes.²² Nowadays, the inversion of configuration around a central atom, usually carbon, is called Walden inversion, which has become probably the best-known reaction mechanism in organic chemistry. S_N2 reactions usually proceed with Walden inversion, initialized by a backside attack such as, for example



where X^- is the nucleophile, and Y is the leaving group. A frontside attack retention mechanism of S_N2 reactions also exists, which is less known, but it was described long time ago²² as



The stationary points along the above-described S_N2 pathways were extensively studied in the past couple of decades.^{23–30} However, as Hase and co-workers¹¹ showed in the case of the $\text{OH}^- + \text{CH}_3\text{F}$ reaction, trajectories may avoid a deep minimum; thus, a dynamical description is needed to understand the complicated chemistry of S_N2 reactions. As mentioned above, the dynamics and mechanisms of S_N2 reactions have been widely studied by direct dynamics simulations, which uncovered several interesting pathways of S_N2 reactions, such as hydrogen-bonded complex formation,¹² rebound,¹³ stripping,¹³ roundabout,³¹ etc., mechanisms. Furthermore, in 2008 Wester and co-workers³¹ developed a crossed-beam technique to measure S_N2 reactions under single-collision conditions, thereby mapping the scattering angle and product internal energy distributions. These new measurements opened the door for direct comparisons between experiments and trajectory simulations. The current status of direct dynamics studies and crossed-beam experiments of S_N2 reactions was recently reviewed by the Hase and Wester groups.^{14,32–35} Here we describe a different theoretical approach to S_N2 reactions based on ab initio analytical PESs. Development of an accurate global analytical PES is a

challenging and time-consuming task, but once the analytical PES is at hand, our approach has several advantages such as (a) the PES may be based on high level of electronic structure theory, for example, explicitly correlated coupled cluster with tripe-zeta basis sets, (b) millions of trajectories can be efficiently computed for any isotopologues, and (c) quantum dynamics studies, at least in reduced dimensions, can be performed. As a consequence of (a) better agreement with experiment and more definitive predictions can be achieved and due to (b) statistically more accurate results, for example, differential cross sections, can be obtained, and new low-probability reaction pathways can be revealed. In Section II we describe the details of the analytical PES development from the choice of the ab initio method and basis to the fitting and the properties of the PESs. In Section III we show examples for all the above-described advantages of our approach in the case of the $\text{F}^- + \text{CH}_3\text{Y}$ [$\text{Y} = \text{F}, \text{Cl}, \text{I}$] reactions. The paper ends with Summary and Conclusions in Section IV also highlighting possible future research directions.

II. AB INITIO ANALYTICAL POTENTIAL ENERGY SURFACES

As mentioned in Section I, the key of our approach is the development of analytical PESs for S_N2 reactions. The main steps of this procedure are the selection of the geometries that cover the configuration space of chemical importance, the ab initio computations at the selected structures, and the fitting of the ab initio energy points. Below we give the details of the above steps along with the specifics for the $\text{F}^- + \text{CH}_3\text{Y}$ [$\text{Y} = \text{F}, \text{Cl}, \text{I}$] reactions.

II.A. Ab Initio Energy Points. The selection of the nuclear configurations plays a key role in the PES development procedure. We apply the combination of the following strategies:

- (1) We set up n -mode grids along the most important $n = 1, 2$, perhaps 3 or 4 internal coordinates keeping the other internal coordinates fixed at stationary-point values.
- (2) Random displacements of the Cartesian coordinates of known stationary points of the system.

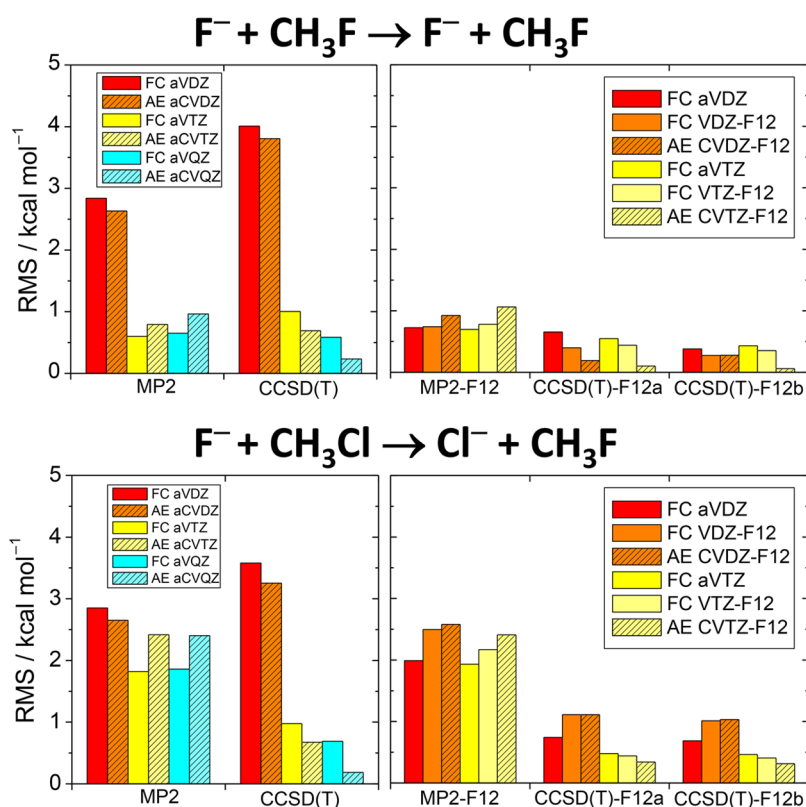


Figure 2. RMS errors of different standard and explicitly correlated F12 ab initio levels of theory for the $F^- + CH_3Y$ [$Y = F, Cl$] S_N2 reactions. For more details see ref 36. Adapted from ref 36. Copyright 2014 American Chemical Society.

- (3) Structures are generated for each individual reactant and product species, and the fragments corresponding to the same channel are placed far, for example, ~ 10 Å, from each other, thereby ensuring the correct asymptotic behavior of the PES.
- (4) After the first fit, one can run trajectories on the PES, and new points can be added to the database along selected trajectories. The analytical PES can be iteratively improved until all the trajectories become physically correct and/or the dynamical simulation gives converged cross sections, reaction probabilities, etc.

The accuracy of the analytical PES depends on the accuracy of the fitting and that of the ab initio level of theory. The former can be checked based on the root-mean-square (RMS) error of the fitting. For the latter we performed a detailed study testing the accuracy of different ab initio methods and basis sets at 15 selected structures, sometimes far from stationary points, for each of the six reactions, $X + CH_4$ [$X = F, O, Cl$] and $F^- + CH_3Y$ [$Y = F, Cl, OH$].³⁶ Representative results showing the accuracy of different standard and explicitly correlated MP2 and CCSD(T) methods^{3,37–39} and double- (DZ), triple- (TZ), and quadruple- ζ (QZ) basis sets^{40,41} are shown in Figure 2 for the $F^- + CH_3Y$ [$Y = F, Cl$] reactions. The main conclusions can be summarized as³⁶

- (1) MP2 with DZ bases has an average accuracy of ~ 3 kcal mol^{-1} .
- (2) TZ and QZ basis sets do not always improve the accuracy of the MP2 method significantly.
- (3) Standard CCSD(T) with DZ bases performs poorly with ~ 3 – 4 kcal mol^{-1} average error.
- (4) Standard CCSD(T) with TZ bases has approximate chemical accuracy of ~ 1 kcal mol^{-1} .

- (5) The explicitly correlated F12 methods^{38,39} converge rapidly, and the CCSD(T)-F12 methods³⁹ give chemical accuracy even with a DZ basis.

We showed that composite approaches, such as A/small + B/large – B/small, where A and B are an expensive and a cheap method, respectively, and small and large denote the size of the basis sets, can be useful, especially in the case of standard methods. The above composite expression relies on the facts that basis set effects have little method dependence and/or the higher-order correlation energy contributions can be well-estimated using small basis sets. Furthermore, we found that electron correlation can have a large effect of ~ 5 – 10 kcal mol^{-1} for S_N2 reactions, core correlation contributions are ~ 0.3 kcal mol^{-1} , and scalar relativistic effects are usually less than 0.1 kcal mol^{-1} .

We reported¹⁶ our first S_N2 analytical PES for the $F^- + CH_3Cl$ reaction in 2013 based on 36 736 composite ab initio energy points obtained as

$$\begin{aligned} & \text{CCSD(T)/aug-cc-pVDZ} + \text{MP2/aug-cc-pVQZ} \\ & - \text{MP2/aug-cc-pVDZ} + (\text{AE-MP2/aug-cc-pCVTZ} \\ & - \text{FC-MP2/aug-cc-pCVTZ}) \end{aligned} \quad (3)$$

where in parentheses the core correlation effect is given as difference between all-electron (AE) and frozen-core (FC) energies. Equation 3 gives AE-CCSD(T)/aug-cc-pCVQZ-quality results with only 0.35 kcal mol^{-1} RMS deviation. In 2015 we reported¹⁷ a new version of the $F^- + CH_3Cl$ PES based on 52 393 energy points, ab initio level of eq 3, which has an improved accuracy at the high-energy region thereby

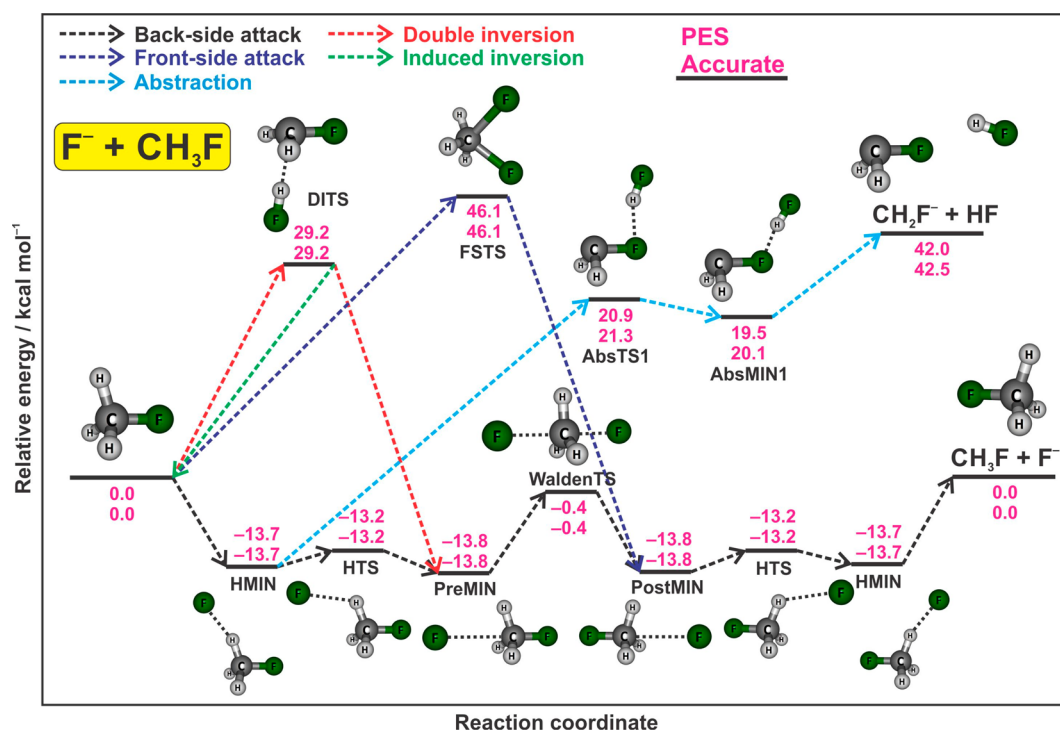
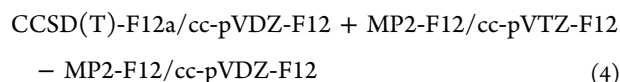


Figure 3. PES of the $F^- + CH_3F$ reaction showing the stationary points and their classical relative energies obtained from the analytical PES and by an accurate relativistic all-electron CCSDT(Q)/complete-basis-set-quality composite ab initio method along the different reaction pathways.¹⁸

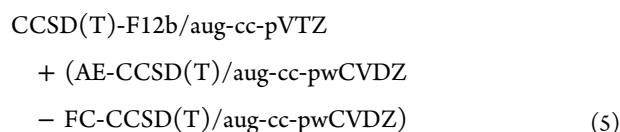
providing a good description of the retention pathways and the proton-transfer channel.

In 2015 we developed¹⁸ a global accurate PES for the $F^- + CH_3F$ reaction using 49 166 explicitly correlated ab initio energy points computed as



Equation 4 was shown to agree with the AE-CCSD(T)-F12b/cc-pCVQZ-F12 data within 0.33 kcal mol⁻¹ on average, thereby outperforming standard CCSD(T) with aug-cc-pVDZ, aug-cc-pVTZ, and aug-cc-pVQZ, which give RMS errors of 4.01, 1.00, and 0.59 kcal mol⁻¹, respectively.

In 2017 we reported¹⁹ a high-level analytical PES for the $F^- + CH_3I$ reaction by fitting 50 496 ab initio energy points obtained as



where the core-correlation effect is given in parentheses, and a relativistic small-core pseudopotential (PP) and the corresponding PP basis set⁴² is used for iodine.

II.B. Fitting the ab Initio Data. PESs must be invariant under (a) translation, (b) rotation, and (c) permutation of the identical atoms. Interatomic coordinates r_{ij} obviously fulfill (a) and (b) and form a closed set under (c). Therefore, we use Morse-type variables $y_{ij} = \exp(-r_{ij}/a)$ to represent PESs, where a is a real fixed parameter. Even if Morse-type variables of all the interatomic coordinates are redundant for more than four-atomic systems, the use of these variables is advantageous for describing the correct asymptotic behavior and satisfying all the

conditions (a)–(c). The PES can be given in the functional form^{43,44}

$$V = \sum_{\mathbf{n}=0}^N C_{\mathbf{n}} \mathcal{S}(y_{12}^{n_{12}} y_{13}^{n_{13}} y_{14}^{n_{14}} \dots y_{23}^{n_{23}} y_{24}^{n_{24}} \dots) \quad (6)$$

where \mathcal{S} is a so-called symmetrization operator,^{43,44} which makes the fitting basis explicitly invariant under permutation of identical atoms, and $C_{\mathbf{n}}$ [$\mathbf{n} = (n_{12}, n_{13}, n_{14}, \dots, n_{23}, n_{24}, \dots)$] denotes the coefficients, which are determined by a weighted linear least-squares fit to the ab initio data. The actual implementation uses the sophisticated permutationally invariant polynomial theory,^{43,44} which makes the evaluation of the PES numerically more efficient. The number of terms (coefficients) in eq 6 depends on the number of atoms, the permutational symmetry, and the maximum order of the polynomials, D , constraining the sum of the exponents in eq 6 less than or equal to D .

For the $F^- + CH_3Y$ [$Y = \text{Cl}, \text{I}$] systems^{16,17,19} we performed fifth-order fits resulting in 3313 coefficients, whereas for $F^- + CH_3F$ (ref 18) a sixth-order fit was done providing 5850 coefficients. Note that, for $F^- + CH_3Y$ [$Y = \text{Cl}, \text{I}$], a sixth-order fit would have given 10 831 coefficients due to the lower permutational symmetry. A weight of $E_0/(E + E_0)$ was used to suppress the less-important high-energy points, where E is the energy relative to the global minimum. E_0 was 0.05 E_h (31 kcal mol⁻¹) for $F^- + CH_3Y$ [$Y = \text{F}, \text{Cl}$] and 0.1 E_h (63 kcal mol⁻¹) for the more exothermic $F^- + CH_3I$. The a parameter, which controls the asymptotic behavior of the PES, was chosen to be 3 bohr in all cases. Note that in atom + CH_4 reactions¹⁰ a smaller a value of 2 bohr, that is, faster decaying basis functions, is used. For S_N2 reactions, where the long-range ion–dipole interactions are important, a more diffuse basis, that is, a larger a parameter, is necessary. The RMS errors of the fittings are

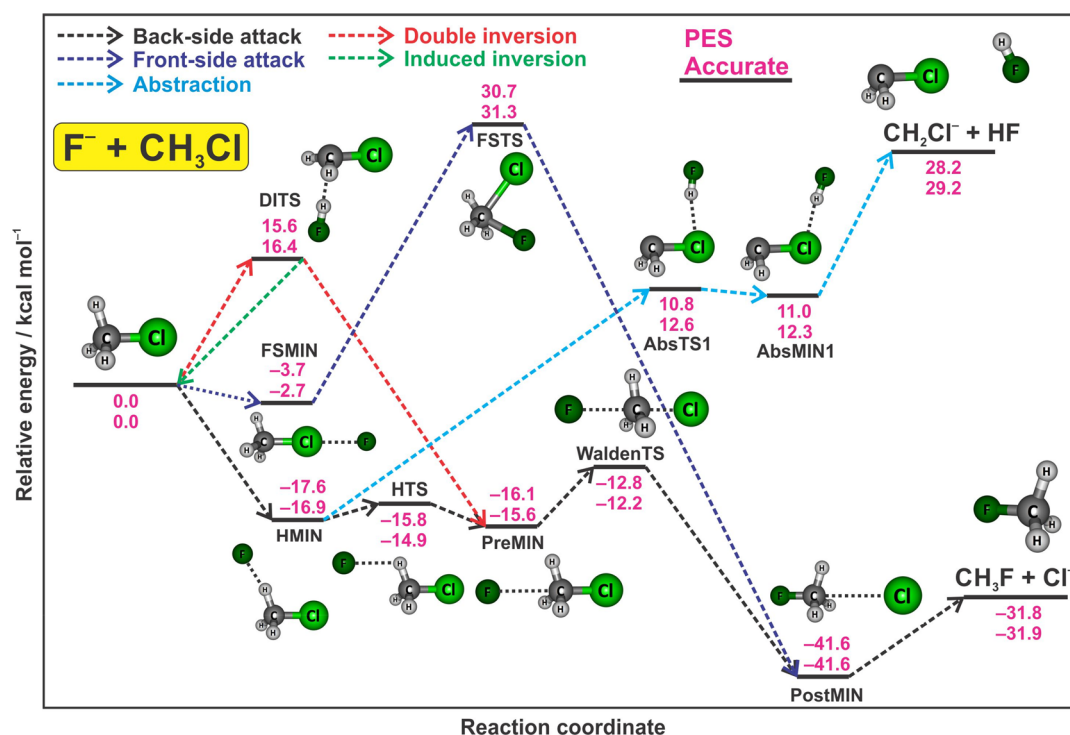


Figure 4. PES of the $F^- + CH_3Cl$ reaction showing the stationary points and their classical relative energies obtained from the analytical PES and by an accurate relativistic all-electron CCSDT(Q)/complete-basis-set-quality composite ab initio method along the different reaction pathways.¹⁷ For details on FSMIN, where the accurate energy is obtained by CCSD(T)-F12b/aug-cc-pVTZ, see ref 50.

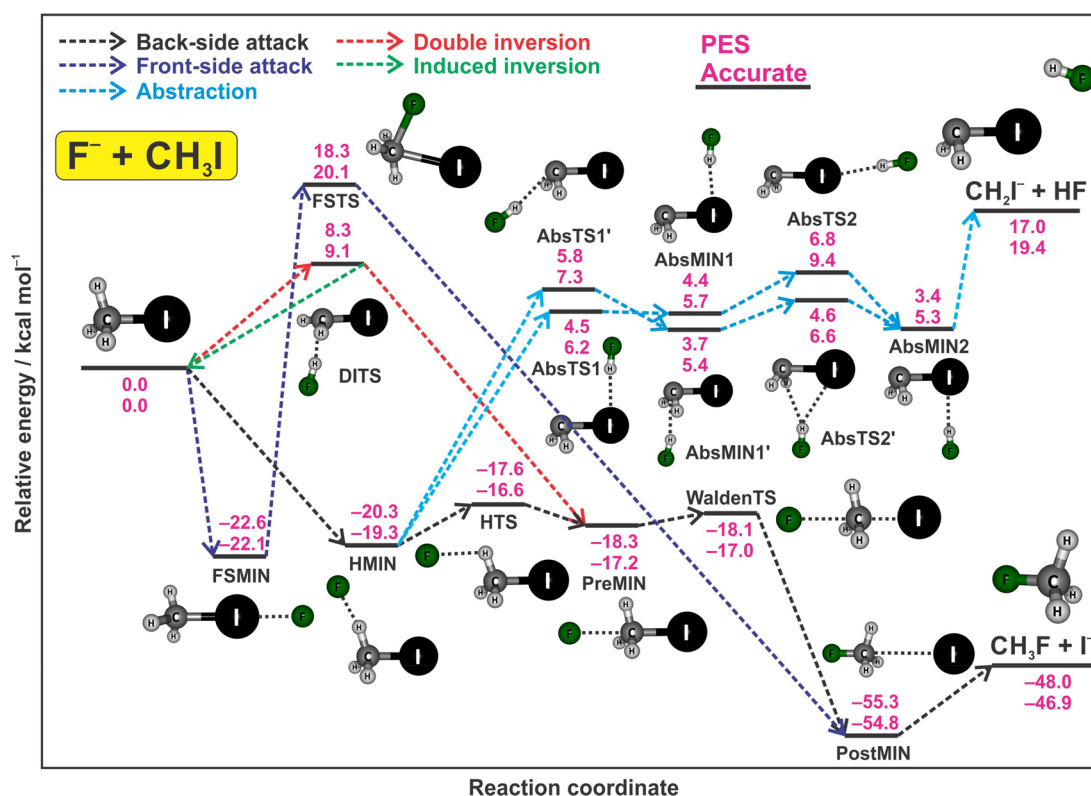


Figure 5. PES of the $F^- + CH_3I$ reaction showing the stationary points and their classical relative energies obtained from the analytical PES and by an accurate all-electron CCSD(T)-F12b/QZ-quality composite ab initio method along the different reaction pathways.¹⁹

usually (well) below 1 kcal mol^{-1} , chemical accuracy, in the chemically important energy ranges.

II.C. Properties of the Potential Energy Surfaces. The potential energy diagrams of the $F^- + CH_3Y$ [$Y = F, Cl, I$] reactions showing the stationary points and their relative

energies along the different reaction pathways are given in Figures 3–5. As seen, the relative energies obtained from the analytical PESs usually agree within 1 kcal mol⁻¹ with the high-level benchmark values. We computed these classical benchmark energies utilizing the composite focal-point analysis approach^{45,46} consisting of CCSD(T)/complete-basis-set results obtained from either extrapolations or explicitly correlated F12 computations with large basis sets, core correlation effects, and sometimes post-CCSD(T) corrections.

All the F⁻ + CH₃Y [Y = F, Cl, I] S_N2 reactions have a double-well PES featuring pre- and postreaction complexes and a transition state (TS) separating the reactants from the products along the Walden-inversion backside attack pathway. Note that in our definition the backside attack mechanism involves the direct rebound and stripping channels as well as the many indirect complex-forming and roundabout inversion pathways. The Walden TS of F⁻ + CH₃F is just slightly below the reactant asymptote by 0.4 kcal mol⁻¹, whereas for F⁻ + CH₃Y [Y = Cl, I] these TSs are significantly submerged by 12.2 and 17.0 kcal mol⁻¹, respectively. In the entrance channel, besides the well-known C_{3v} ion–dipole complexes, F⁻⋯H₃CY, with depths of 13.8, 15.6, and 17.2 kcal mol⁻¹ for Y = F, Cl, and I, respectively, hydrogen-bonded C_s complexes below the reactants by 13.7, 16.9, and 19.3 kcal mol⁻¹, respectively, are also found. For Y = F the energies of the C_{3v} and C_s complexes are nearly identical, but for Y = Cl and I the H-bonded complex is clearly slightly more stable. We found first-order saddle points separating these minima by low barriers of 0.5/0.6, 2.0/0.7, and 2.7/0.6 kcal mol⁻¹ relative to the C_s/C_{3v} minima for Y = F, Cl, and I, respectively. Note that H-bonded complex was also previously found for OH⁻ nucleophile,⁴⁷ and perhaps surprisingly we recently obtained a H-bonded complex for the Cl⁻ + CH₃I reaction as well,⁴⁸ albeit here the ion–dipole minimum is slightly deeper. Furthermore, for the F⁻ + CH₃I reaction we found a C_{3v} frontside complex, F⁻⋯ICH₃, which is actually the global minimum in the entrance channel with depth of 22.1 kcal mol⁻¹.^{49,50} Similar frontside minimum also exists for Y = Cl, but it is much shallower, only ~3 kcal mol⁻¹ deep.^{49,50}

As already shown in eq 2, there is a frontside attack retention pathway via high barriers of 46.1, 31.3, and 20.1 kcal mol⁻¹ for F⁻ + CH₃Y, where Y = F, Cl, and I, respectively. In the case of F⁻ nucleophile the frontside TSs have C_s symmetry with FCY angles of ~80°. However, for Y = F the two F atoms are out of the C_s plane, whereas for Y = Cl, I, and Br four atoms, namely, H, C, F, Y, are in the C_s plane.⁵¹

In 2015 we reported a double-inversion TS for the F⁻ + CH₃Cl S_N2 reaction based on reaction dynamics simulations.¹⁷ As the trajectories showed the first step of double inversion is a proton abstraction induced inversion via a FH⋯CH₂Y⁻ TS (C_s symmetry), which is eventually followed by a second inversion through the traditional Walden TS resulting in overall retention. As Figures 3–5 show for F⁻ + CH₃Y the double-inversion barrier heights of 29.2, 16.4, and 9.1 kcal mol⁻¹ for Y = F, Cl, and I, respectively, are well-below the corresponding frontside attack barriers. Note that recent studies show that intrinsic reaction coordinate (IRC) computations do not connect the above-described double-inversion TS to the double-inversion reaction path suggesting non-IRC dynamics.^{52,53} Indeed, the majority of the trajectories initiated from the double-inversion TS lead to S_N2 products with double inversion.⁵³ More discussion on this novel mechanism is given in Section III.

Besides the S_N2 channel, proton abstraction (proton transfer) leading to HF + CH₂Y⁻ can also occur in the F⁻ + CH₃Y reactions. Proton transfer is endothermic, ΔE = 42.5, 29.2, and 19.4 kcal mol⁻¹ for Y = F, Cl, and I, respectively, barrierless process involving many stationary points below the product asymptote. In our earlier studies on F⁻ + CH₃Y [Y = F, Cl] we only identified two stationary points along the proton-transfer pathway.^{17,18} Motivated by Hase and co-workers,⁵² for F⁻ + CH₃I our PES describes many proton-transfer minima and saddle points as shown in Figure 5.¹⁹ In 2017 we also reported similar stationary points for the Cl⁻ + CH₃I reaction as well.⁴⁸ Finally we note that in the case of F⁻ nucleophile the energy of the HF + CH₂Y⁻ products is always above the corresponding double-inversion TS; thus, double inversion can be expected at collision energies below the threshold of the proton abstraction channel.

III. REACTION DYNAMICS SIMULATIONS

Utilizing the analytical PESs we can perform efficient quasi-classical trajectory (QCT) and/or reduced-dimensional quantum dynamics computations for the F⁻ + CH₃Y [Y = F, Cl, I] reactions. Our QCT studies usually consider millions of, sometimes over 10 million, trajectories, thereby providing unprecedented statistical accuracy for S_N2 reactions, revealing novel minor reaction pathways, and allowing the computation of mode-specific product vibrational distributions. The product vibrational-state assignments are performed by using the normal-mode analysis procedure, and the mode-specific distributions are obtained by the energy-based one-dimensional Gaussian binning (1GB) technique as described in detail in refs 54, 55, and 56. 1GB, which was proposed by one of us in 2009,⁵⁴ incorporates some quantum effects into the QCT product analysis by weighting the trajectories based on the energy difference between the actual classical vibrational energy and the corresponding quantum level of the product molecules. The 1GB method has been successfully applied for many systems such as atom + methane,¹⁰ OH + D₂,^{57,58} CO,⁵⁹ CHD₃,⁶⁰ (H₂O)₂ → 2H₂O,^{61,62} etc., and we reported its first applications for S_N2 reactions.^{16,56}

There have been many studies on the dynamics of S_N2 reactions in the literature whose review is out of the scope of this Feature Article. Instead, below we focus on our novel results on different mechanisms, vibrational and rotational mode specificity, the highest-dimensional quantum dynamics, comparison with detailed cross-beam experiments, where the new high-level ab initio global analytical PESs play key roles.

III.A. Walden Inversion of S_N2 Reactions. The Walden-inversion cross sections of the exothermic S_N2 reactions, such as F⁻ + CH₃Y [Y = Cl, I], decrease with increasing collision energy (E_{coll}) as shown in Figure 6. To gain more insight we computed the initial attack angle distributions at different collision energies, as shown in Figure 7 for the F⁻ + CH₃Cl reaction.¹⁶ Attack angle is defined at the beginning of the trajectories as the angle between the velocity vector of the center of mass of CH₃Cl and the C–Cl bond axis. As Figure 7 shows, at higher collision energies the backside attack, that is, F⁻ attacks the CH₃ side of the CH₃Cl molecule, clearly dominates, whereas at low collision energies, for example, 1 kcal mol⁻¹, the initial attack angle distributions are almost isotropic with only a slight backside preference. This shows that at low collision energies the initial orientation does not matter, because the long-range attractive ion–dipole interactions can steer the reactants into a reactive backside orientation even if

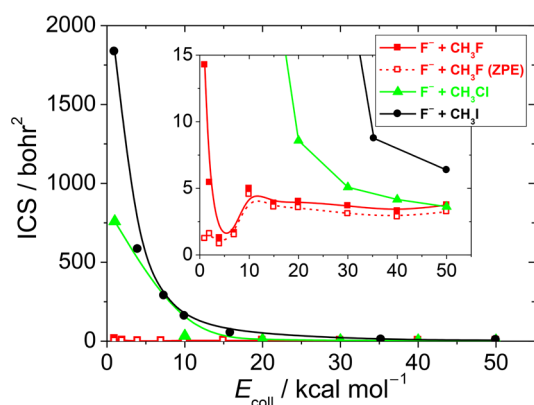


Figure 6. Cross sections of the $F^- + CH_3Y$ [$Y = F, Cl, I$] S_N2 reactions as a function of collision energy obtained without ($Y = F, Cl, I$) and with ($Y = F$) ZPE constraint.^{18,17,19}

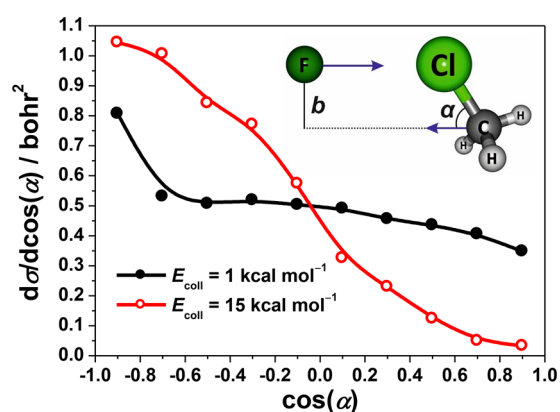


Figure 7. Normalized initial attack angle distributions for the $F^- + CH_3Cl$ S_N2 reaction at collision energies of 1 and 15 kcal mol⁻¹.¹⁶

the F^- initially approaches the frontside, Cl side, of the CH_3Cl molecule. This steering effect obviously diminishes as E_{coll} increases resulting in decreasing cross sections.

As Figure 6 shows the collision energy dependence of the $F^- + CH_3F$ S_N2 cross sections is somewhat different from that of the above-described exothermic reactions. For the isoenergetic $F^- + CH_3F$ reaction the product zero-point energy (ZPE) violation is significant at low E_{coll} . Without ZPE constraint the cross sections have a “Morse-curve-like” shape, that is, large values at very low E_{coll} , minimum at $E_{coll} \approx 4$ kcal mol⁻¹, and a constant value at high E_{coll} whereas the ZPE constraint significantly reduces the reactivity at very low E_{coll} , resulting in cross sections of ~ 1 – 2 bohr², which increase with E_{coll} and reach a nearly constant value of ~ 4 bohr² at E_{coll} of ~ 10 kcal mol⁻¹.

Since the $F^- + CH_3F$ S_N2 reaction has a symmetric double-well potential, where the central TS, which separates the two ~ 14 kcal mol⁻¹ deep wells, is only slightly, 0.4 kcal mol⁻¹, below the energy levels of the reactants and products, we can expect significant recrossing dynamics. Figure 8 shows the cross sections as a function of the number of TS crossings at different collision energies. Odd number of crossings means reactive trajectories, whereas even number of crossings corresponds to non-reactive events. As seen, a significant number of trajectories cross the barrier twice, resulting in an $\sim 20\%$ decrease of the reactivity relative to a simple transition-state theory picture, which does not consider the possibility of recrossing.

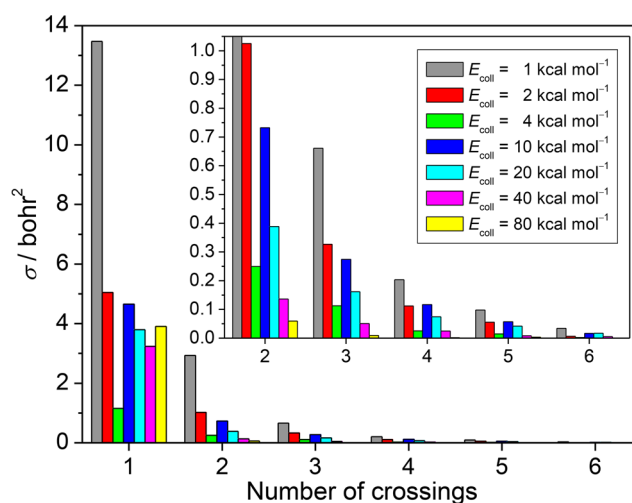


Figure 8. Integral cross sections of the $F^- + CH_3F$ S_N2 reaction as a function of the number of saddle-point crossings at different collision energies. Adapted from ref 18. Copyright 2015 American Institute of Physics.

Interestingly the recrossing probability is found to be substantial even at higher collision energies.

Walden inversion can occur via direct rebound, direct stripping, and indirect mechanisms resulting in fingerprints in the scattering angle distributions in the backward, forward, and isotropic directions, respectively.¹⁶ Indirect trajectories involve long-lived complex formation, which can be significant at low E_{coll} and diminishes as E_{coll} increases; thus, one may expect a transition from indirect to direct dynamics with increasing E_{coll} . However, as our recent studies show, the picture is not so simple, because the leaving group can significantly influence the dynamics of S_N2 reactions.^{49,50} In 2016 our joint experimental–theoretical study⁴⁹ found that the $F^- + CH_3Cl$ reaction is more direct (i.e., direct rebound dominates over the indirect mechanisms) than the seemingly similar $F^- + CH_3I$ S_N2 reaction. We speculated that frontside complex formation may explain this intriguing leaving-group effect, since as mentioned in Section II, the $F^- + CH_3I$ reaction has a deep frontside minimum with depth of 22.1 kcal mol⁻¹, whereas the corresponding $F^- \cdots ClCH_3$ minimum is only ~ 3 kcal mol⁻¹ deep. Thus, on one hand, one may expect that the deep $F^- \cdots ICH_3$ minimum steers the $F^- + CH_3I$ trajectories away from the reactive $F^- \cdots H_3CI$ orientation corresponding to a 17.2 kcal mol⁻¹ deep minimum, thereby making the reaction more indirect. On the other hand, in the case of $F^- + CH_3Cl$ the shallow ~ 3 kcal mol⁻¹ deep frontside minimum does not significantly influence the orientation effect of the 15.6 kcal mol⁻¹ deep backside minimum, which enhances the direct rebound reactions. In 2017 when we had analytical PESs for both the $F^- + CH_3Y$ [$Y = Cl, I$] systems, we could verify the above hypothesis based on dynamical simulations.⁵⁰ We developed a method called trajectory orthogonal projection (TOP), which projects the position of the nucleophile to one-dimensional (1D; C–Y bond axis) or two-dimensional (2D; Y–C–H plane) subspaces and determines its spatial distributions in the entrance channel. The TOP graphics of Figure 9 show significant frontside complex formation for the $F^- + CH_3I$ reaction, whereas virtually only backside complex formation is seen for $F^- + CH_3Cl$, supporting the above-described assumptions. It is also worth noting that the two-dimensional TOP distributions nicely show the H-bonded complex

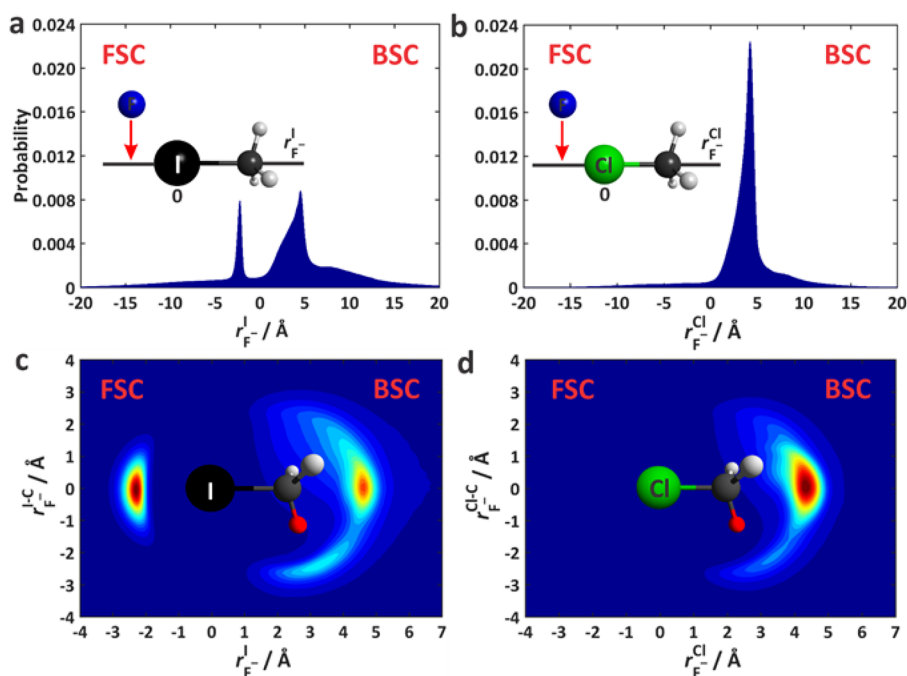


Figure 9. Normalized spatial distributions of the F^- nucleophile around CH_3Y [$Y = Cl, I$] on the reactant side of the $F^- + CH_3Y$ S_N2 reactions at the collision energy of 1 kcal mol^{-1} obtained by 1D (a, b) and 2D (c, d) trajectory orthogonal projection to the $\{C,Y\}$ line and to the $\{Y,C,H$ (red) $\}$ plane as indicated by the structures, respectively. Adapted from ref 50. Copyright 2017 American Chemical Society.

formation in both cases. To the best of our knowledge, these are the first simulations that quantitatively show frontside complex formation in S_N2 reactions based on millions of trajectories and billions of nuclear configurations (hundreds of gigabytes of data).

III.B. Double-Inversion and Front-Side Attack S_N2 Retention Mechanisms. In 2013 we implemented a method that can numerically determine the configuration of the product molecule relative to that of the reactant. (Note that in a QCT simulation each H atom can be labeled; thus, we can distinguish between “stereoisomers” of methyl halides.) We applied this analysis method to the $F^- + CH_3Cl$ trajectories, and besides many inverted products we found CH_3F molecules with retention of the initial configuration. Of course, this is not unexpected, because a frontside attack retention mechanism of S_N2 reactions, see eq 2, has been known for a long time. However, the fact that we found retention trajectories at collision energies well below the barrier height of the frontside attack pathway was really surprising. Examination of the relevant trajectories revealed a new S_N2 retention mechanism, which received the name of double inversion.¹⁷ As Figure 10 shows, first F^- abstracts a proton from CH_3Cl , but the HF fragment does not have enough energy to dissociate and instead starts the move around the CH_2Cl^- unit, and eventually the proton bonds back to the carbon atom resulting in a first inversion, which is followed by a second inversion via the usual Walden-TS. The two inversions, that is, a double inversion, result in overall retention. Since double inversion is a slow indirect process, the corresponding scattering angle distributions are nearly isotropic, whereas the frontside attack is more direct resulting in dominance of sideway scattering in accord with the corresponding TS structure ($F-C-Cl$ angle is 81°).¹⁷

On the basis of the double-inversion trajectories we found a $FH\cdots CH_2Cl^-$ -type TS (C_s symmetry), which was called double-inversion TS.¹⁷ Later we identified similar double-inversion TSs

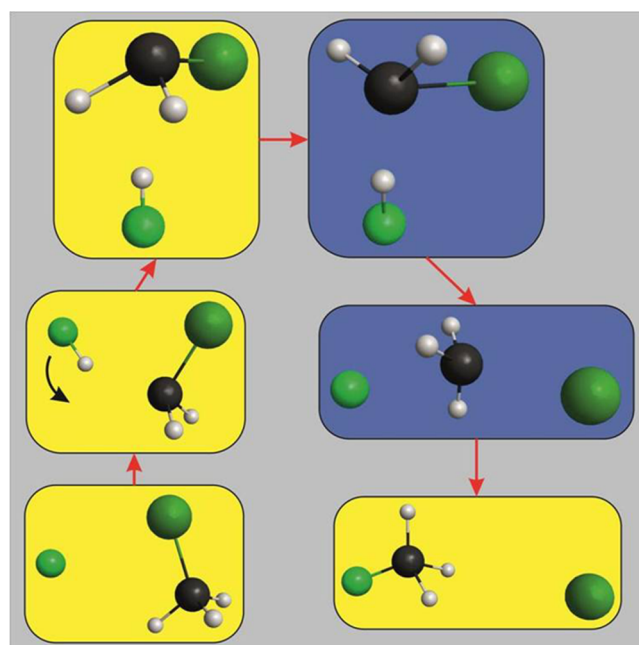


Figure 10. Double-inversion mechanism of the $F^- + CH_3Cl$ S_N2 reaction.¹⁷

for all the $16 X^- + CH_3Y$ [$X,Y = F, Cl, Br, I$] reactions showing that double inversion can be a general mechanism of S_N2 reactions.⁵¹ Indeed, recently we found double-inversion trajectories for the $F^- + CHD_2Cl$ (ref 56), $F^- + CH_3F$ (ref 18), and $F^- + CH_3I$ (ref 19) S_N2 reactions, as well. As Figure 11 shows the double-inversion TS is below the corresponding frontside attack TS for F^- nucleophile, and the reverse holds for $X = Cl, Br,$ and I .⁵¹ The proton abstraction product asymptotes ($HX + CH_2Y^-$) are above the corresponding double-inversion TSs in all the cases, showing that double inversion can occur at

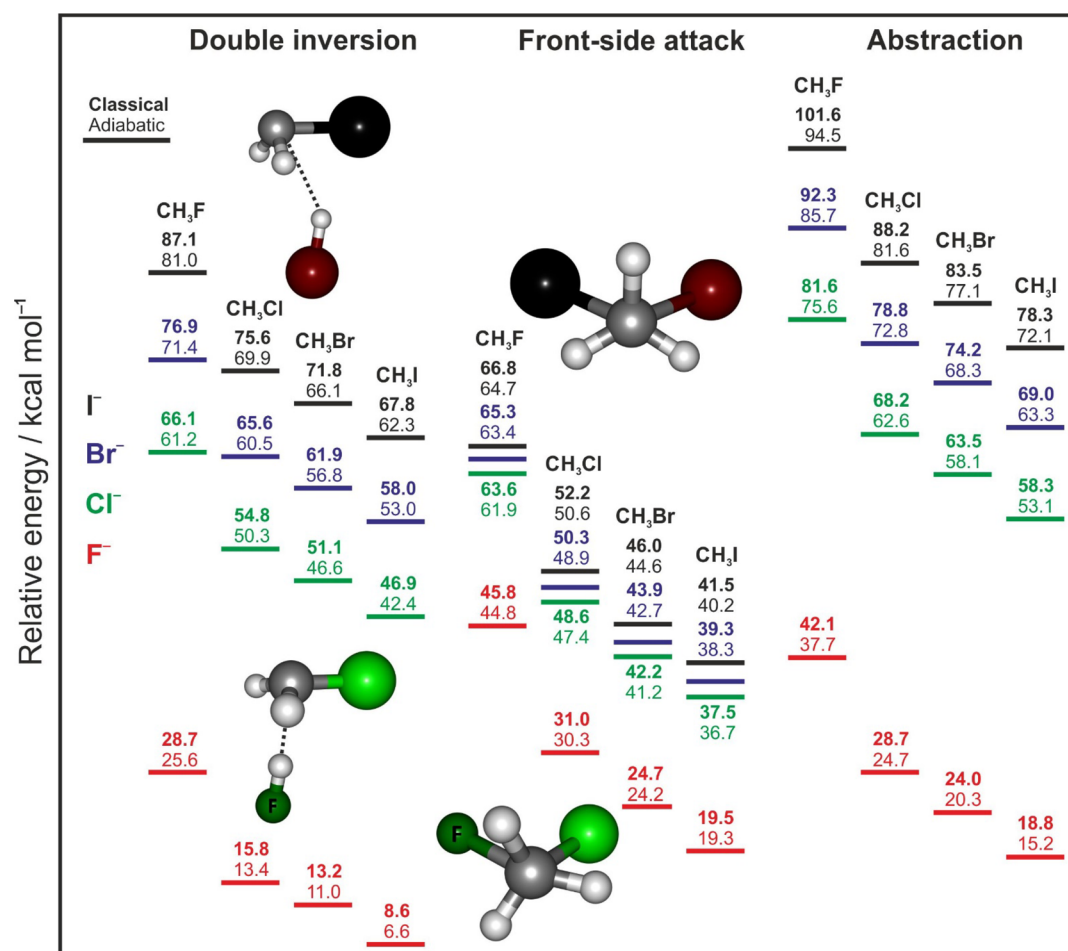


Figure 11. Classical and ZPE-corrected (adiabatic) energies of the double-inversion and frontside attack TSs and abstraction-channel products (HX + CH₂Y⁻) relative to the energies of the reactants, X⁻ (color coded) + CH₃Y (columns), obtained at the CCSD(T)-F12b/aug-cc-pVTZ(-PP) level of theory. Adapted from ref 51. Copyright 2015 American Chemical Society.

collision energies below the abstraction thresholds. The lowest double-inversion barrier height is found for F⁻ + CH₃I; thus, we expected the highest double-inversion probability for this reaction among the halide ion + methyl-halide systems. Our assumption that the double-inversion reactivity is higher in F⁻ + CH₃I than in F⁻ + CH₃Cl was later confirmed by QCT simulations.¹⁹ Figure 12 shows the double-inversion cross sections for F⁻ + CH₃Y [Y = Cl, I] as a function of collision energy. As seen, the cross sections are larger for Y = I, and the maxima of the excitation functions shift from $E_{\text{coll}} = \sim 30$ to ~ 15 kcal mol⁻¹ for Y = Cl and I, respectively. The absolute double-inversion cross sections are comparable with those of the H + CH₄ reaction, even if the retention cross sections relative to the Walden-inversion ones are small (1–2%).

The discovery of the double-inversion mechanism of S_N2 reactions has motivated experts in the field to study this phenomenon. Wang and co-workers^{63,64} identified a double-inversion reaction pathway in aqueous solution for the F⁻ + CH₃Cl and F⁻ + CH₃I S_N2 reactions. Hase and co-workers⁵² investigated the double-inversion TS of F⁻ + CH₃I and concluded that double inversion may be a non-IRC process. Later they performed direct dynamics computations initiated from the so-called double-inversion TS and found that $\sim 70\%$ of the trajectories follow the above-described double-inversion pathway.⁵³ Finally we note that we found a double-inversion TS

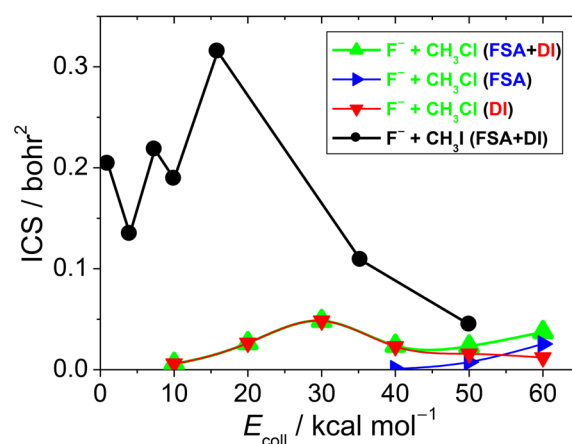


Figure 12. Retention cross sections via the frontside attack (FSA) and double-inversion (DI) pathways for the F⁻ + CH₃Y [Y = Cl and I] S_N2 reactions as a function of collision energy.^{17,19}

for the F⁻ + CH₃CH₂Cl S_N2 reaction;⁶⁵ thus, this mechanism is expected to exist for larger systems as well.

III.C. Proton-Transfer Channels. Besides the S_N2 channel, the proton abstraction (proton transfer from the neutral reactant to the nucleophile) is an important process in ion–molecule reactions. While the X⁻ + CH₃Y [X, Y = F, Cl, Br, I] S_N2 reactions are exothermic if X < Y, the X⁻ + CH₃Y → HX +

CH_2^- reactions are endothermic as shown in Figure 11. Our analytical PESs developed for $\text{F}^- + \text{CH}_3\text{Y}$ [$\text{Y} = \text{F}, \text{Cl}, \text{I}$] describe the proton-transfer pathway as shown in Figures 3–5. Note that our PES describes many abstraction stationary points for $\text{F}^- + \text{CH}_3\text{I}$; however, most of the corresponding structures are not shown for $\text{F}^- + \text{CH}_3\text{Y}$ [$\text{Y} = \text{F}, \text{Cl}$], because during the earlier PES developments we did not focus on the complete characterization of the proton-transfer region. We determined the cross sections for the proton transfer process for all of the $\text{F}^- + \text{CH}_3\text{Y}$ [$\text{Y} = \text{F}, \text{Cl}, \text{I}$] reactions at several collision energies.^{17–19} The cross sections rapidly increase from threshold energies with increasing E_{coll} . At high E_{coll} (>50 kcal mol⁻¹) the abstraction cross sections have similar magnitude as the $\text{S}_{\text{N}}2$ ones for $\text{F}^- + \text{CH}_3\text{Y}$ [$\text{Y} = \text{Cl}, \text{I}$]. Unlike for the exothermic $\text{S}_{\text{N}}2$ reactions, here the ZPE constraint has a significant effect on the reactivity, that is, decreases the cross sections and shifts up the thresholds to the physically correct values.

In 2016 we reported a detailed QCT study for the abstraction channels of the $\text{F}^- + \text{CHD}_2\text{Cl}$ reaction.⁵⁶ The proton/deuteron transfer was found nonstatistical, since the HF and DF cross sections are almost the same, whereas the statistical ratio would be 1/2. (This finding is not affected by the use of different ZPE constraints.) We managed to distinguish between double-inversion trajectories via either proton or deuteron abstraction-induced inversions. Interestingly, here the cross-section ratios of the proton/deuteron-induced double-inversion trajectories are almost statistical. Correlated initial attack angle and scattering angle distributions reveal three different direct mechanisms for proton/deuteron transfer, that is, backside rebound, backside stripping, and frontside stripping. More discussion of the abstraction process is given in Section IIID.

III.D. Vibrational Mode Specificity. The excitation of specific vibrational modes of the reactants may have substantial effects on the reactivity of polyatomic chemical reactions. This phenomenon is frequently studied in atom plus polyatom reactions, such as $\text{X} + \text{H}_2\text{O}$ and $\text{X} + \text{CH}_4$ [$\text{X} = \text{H}, \text{F}, \text{O}, \text{Cl}$] or isotopologue-analogue systems,^{66–70,10} but less is known about the mode-specific dynamics of $\text{S}_{\text{N}}2$ reactions. We performed detailed QCT computations for the mode-specific dynamics of the $\text{F}^- + \text{CH}_3\text{Cl}(\nu_k = 0,1)$ [$k = 1–6$] and $\text{F}^- + \text{CHD}_2\text{Cl}(\nu_{\text{CH/CD}} = 0,1)$ reactions,^{20,56} preparing the initial vibrational states using standard normal-mode sampling.⁷¹ The $\nu_k = 1/\nu = 0$ cross section ratios as a function of collision energy are shown for the $\text{F}^- + \text{CH}_3\text{Cl}(\nu_k = 0,1)$ $\text{S}_{\text{N}}2$ reactions in Figure 13. As seen, significant mode-specificity is found even if this $\text{S}_{\text{N}}2$ reaction has a submerged barrier. The excitation of the C–Cl stretching mode (ν_3), which increases the cross sections by 10–40% in the E_{coll} interval 1–10 kcal mol⁻¹, has the most substantial effect on the reactivity. The umbrella mode (ν_2) excitation has an enhancement factor of ~0–10%, and the symmetric CH stretching (ν_1) excitation inhibits at low E_{coll} and enhances by 10–20% at higher E_{coll} . This latter CH stretching effect may be overestimated due to the energy leakage from the high-energy excited CH stretching mode to the low-energy modes.

In the case of the CH/CD stretching-excited $\text{F}^- + \text{CHD}_2\text{Cl}(\nu_{\text{CH/CD}} = 1)$ reactions we tested that the reactant maintains the excited $\nu_{\text{CH}}(a') = 1$ character, and significant and slight energy leakages are found for the $\nu_{\text{CD}}(a') = 1$ and $\nu_{\text{CD}}(a'') = 1$ states, respectively.⁵⁶ Nevertheless, our tests show that QCT should be capable to describe at least semi-quantitatively the vibrational effects in methyl-halide reactions.

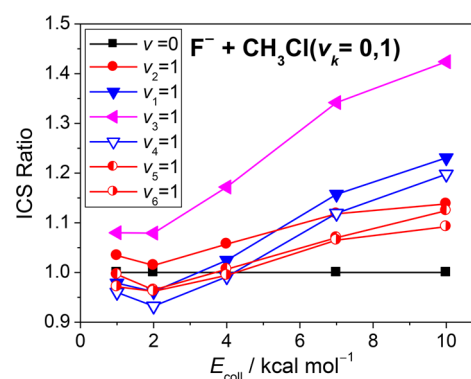


Figure 13. The $\nu_k = 1/\nu = 0$ cross-section ratios for the $\text{F}^- + \text{CH}_3\text{Cl}(\nu_k = 0,1)$ [$k = 1–6$] $\text{S}_{\text{N}}2$ reactions as a function of collision energy obtained by mode-specific QCT computations. Adapted from ref 20. Copyright 2016 American Chemical Society.

In the E_{coll} range of 1–10 kcal mol⁻¹ similar vibrational stretching effects are found for $\text{F}^- + \text{CHD}_2\text{Cl}$ as described above for $\text{F}^- + \text{CH}_3\text{Cl}$. At E_{coll} larger than 10 kcal mol⁻¹, the enhancement factors start to decrease, and the CH/CD excitations even slightly inhibit at high E_{coll} . We also investigated the effect of the initial vibrational excitation on the double-inversion and abstraction pathways. CH and CD stretching excitations are found to clearly enhance both double inversion and proton/deuteron transfer. As expected, the CH stretching excitation enhances the HF channel more substantially than the CD excitations promote the DF abstraction.

Because of the facts that we implemented a methodology to perform mode-specific vibrational analysis for the polyatomic product molecules and the analytical PESs allow the computation of sufficiently large number of trajectories for reasonable statistics, we could determine product vibrational state-specific distributions for $\text{S}_{\text{N}}2$ and proton-transfer reactions.^{16,56} As an example, Figure 14 shows vibrational distributions for the CHD_2F product of the $\text{F}^- + \text{CHD}_2\text{Cl}(\nu_{\text{CH}} = 0,1)$ reactions. These mode-specific results show that even if the probability of excitation on the CH stretching mode of the product increases upon CH stretching excitation of the reactant, the CH stretching is not a pure spectator in this $\text{S}_{\text{N}}2$ reaction.

III.E. Rotational Mode Specificity. We introduced the notion “rotational mode specificity” in 2014 studying the dynamics of the $\text{Cl} + \text{CHD}_3 \rightarrow \text{HCl} + \text{CD}_3$ reaction.⁷² CHD_3 is a symmetric top characterized by rotational quantum numbers J and K . Our joint experimental–theoretical study showed that rotational excitation enhances the above reaction and that specific JK rotational states have different effects on the reactivity; that is, the reaction is rotationally mode specific.⁷² CH_3Y [$\text{Y} = \text{F}, \text{Cl}, \text{Br}, \text{I}$] molecules are also symmetric rotors, where, for nonzero total angular momentum, $K = 0$ classically corresponds to a tumbling motion, and $K = J$ means spinning rotation as shown in Figure 15. In 2015 we studied the rotational mode specific dynamics of the $\text{F}^- + \text{CH}_3\text{Y}(\nu = 0, JK)$ [$\text{Y} = \text{F}, \text{Cl}$] $\text{S}_{\text{N}}2$ reactions.⁷³ Rotational mode specificity is found, though a clear qualitative picture has not emerged. We can say that rotational excitation usually inhibits the $\text{S}_{\text{N}}2$ reactions, and the effect increases with J . Interestingly, the K dependence of the reactivity is different for F and Cl leaving groups. For $\text{F}^- + \text{CH}_3\text{F}$ significant inhibition is found for $K = 0$, where the corresponding effect was negligible for $\text{F}^- + \text{CH}_3\text{Cl}$. For $K = J$ substantial inhibition effects are found in the case of

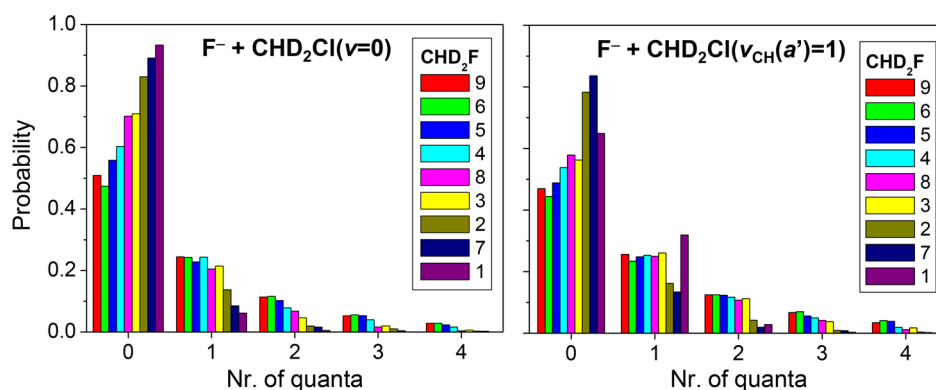


Figure 14. Normalized 1GB distributions of the vibrational quantum states at collision energy of 50 kcal mol^{-1} for the CHD_2F product of the $\text{F}^- + \text{CHD}_2\text{Cl}(v_{\text{CH}}(a') = 0,1)$ $\text{S}_{\text{N}}2$ reactions. Adapted from ref 56. Copyright 2016 American Institute of Physics.

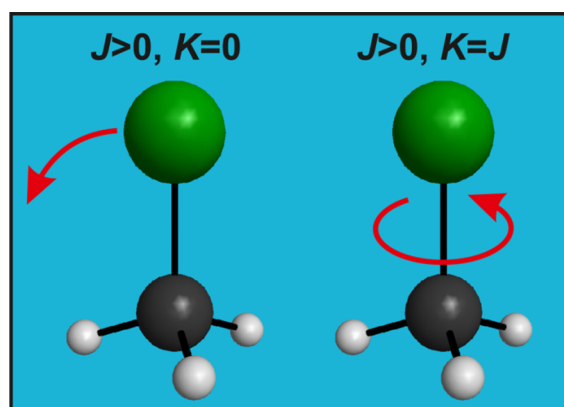


Figure 15. Rotational modes of the CH_3Y [$\text{Y} = \text{F}, \text{Cl}, \text{Br}, \text{I}$] molecules. Adapted from ref 73. Copyright 2015 American Chemical Society.

both reactions. A more detailed analysis of these results can be found in ref 73, but future theoretical and experimental work is clearly needed to formulate a definitive conclusion and explanation on rotational mode specificity in $\text{S}_{\text{N}}2$ reactions.

III.F. Quantum Dynamics. Although high-dimensional quantum dynamical computations are frequently applied to polyatomic reactions such as atoms + water^{74,75} and methane,^{76–80} the quantum studies of $\text{S}_{\text{N}}2$ reactions were restricted to low-, 2–4-dimensional models^{81–85} partially due to the unavailability of full-dimensional PESs. Recently, our full-dimensional analytical PESs opened the door for high-level quantum dynamics simulations for $\text{S}_{\text{N}}2$ reactions. In 2016 we, in collaboration with the Yang and Guo groups, reported the highest-dimensional quantum dynamics study for an $\text{S}_{\text{N}}2$ reaction.²⁰ Time-dependent wave-packet computations were performed for the $\text{F}^- + \text{CH}_3\text{Cl}$ reaction using a six-dimensional model and our ab initio PES. In this non-collinear model the most important vibration modes of the reactant, that is, C–Cl stretching, umbrella, and symmetric CH stretching, were active allowing mode-specific investigations. The quantum computations show that the C–Cl stretching enhances the reactivity the most efficiently, slight enhancement is seen upon umbrella excitation, and CH stretching excitation can inhibit the reaction at larger E_{coll} . Most of these findings are in good agreement with the QCT results, except that QCT shows enhancement upon CH excitation presumably due to the energy leakage issue. As Figure 16 shows, the quantum and QCT reaction probabilities and cross sections are in remarkable agreement, boldfacing that QCT is capable to describe the dynamics of $\text{S}_{\text{N}}2$

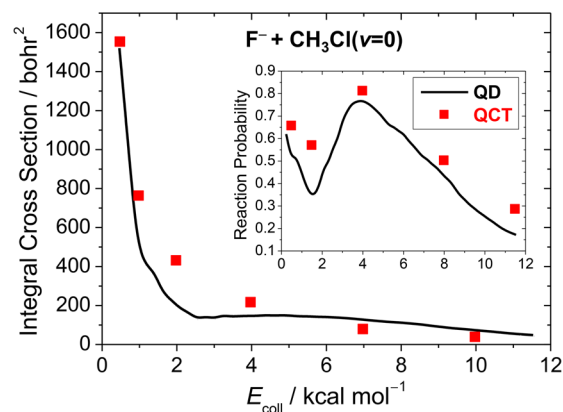


Figure 16. Comparison of the quantum (QD) and classical (QCT) reaction probabilities ($J_{\text{tot}} = 0$) and integral cross sections of the $\text{F}^- + \text{CH}_3\text{Cl}$ $\text{S}_{\text{N}}2$ reaction as a function of collision energy.²⁰

reactions. Recently, Wang and co-workers⁸⁶ also performed quantum dynamics computations on our PES using a four-dimensional model and found good agreement with our previous quantum and QCT results.

III.G. Comparison with Experiments. The crossed-beam studies of Wester and co-workers allow direct comparison between theory and experiment. In 2016 we reported a joint experimental and theoretical investigation on the dynamics of the $\text{F}^- + \text{CH}_3\text{Cl}$ $\text{S}_{\text{N}}2$ reaction.⁴⁹ As Figure 17 shows the agreement between the computed and measured scattering angle and product internal energy distributions is excellent. The analytical PES played a key role in this comparison, because this PES allowed achieving unprecedentedly high statistical accuracy and resolution for these detailed differential cross-section data. The comparison of the results obtained for $\text{F}^- + \text{CH}_3\text{Cl}$ to those of $\text{F}^- + \text{CH}_3\text{I}$ revealed surprising leaving-group effect in $\text{S}_{\text{N}}2$ reactions.⁴⁹ As already discussed in Section IIIA, this finding can be explained by significant frontside complex formation in $\text{F}^- + \text{CH}_3\text{I}$,⁵⁰ which makes this reaction more indirect than $\text{F}^- + \text{CH}_3\text{Cl}$. In 2017 we performed QCT computations for the $\text{F}^- + \text{CH}_3\text{I}$ reaction as well¹⁹ and compared the computed scattering angle and product internal energy distributions to the previous crossed-beam data¹³ as shown in Figure 17. While QCT qualitatively and in some cases semiquantitatively reproduces the measured distributions, some disagreements, especially at higher collision energies, are seen. This motivates us to further improve the theoretical results, which is a work in progress. Nevertheless, the comparisons

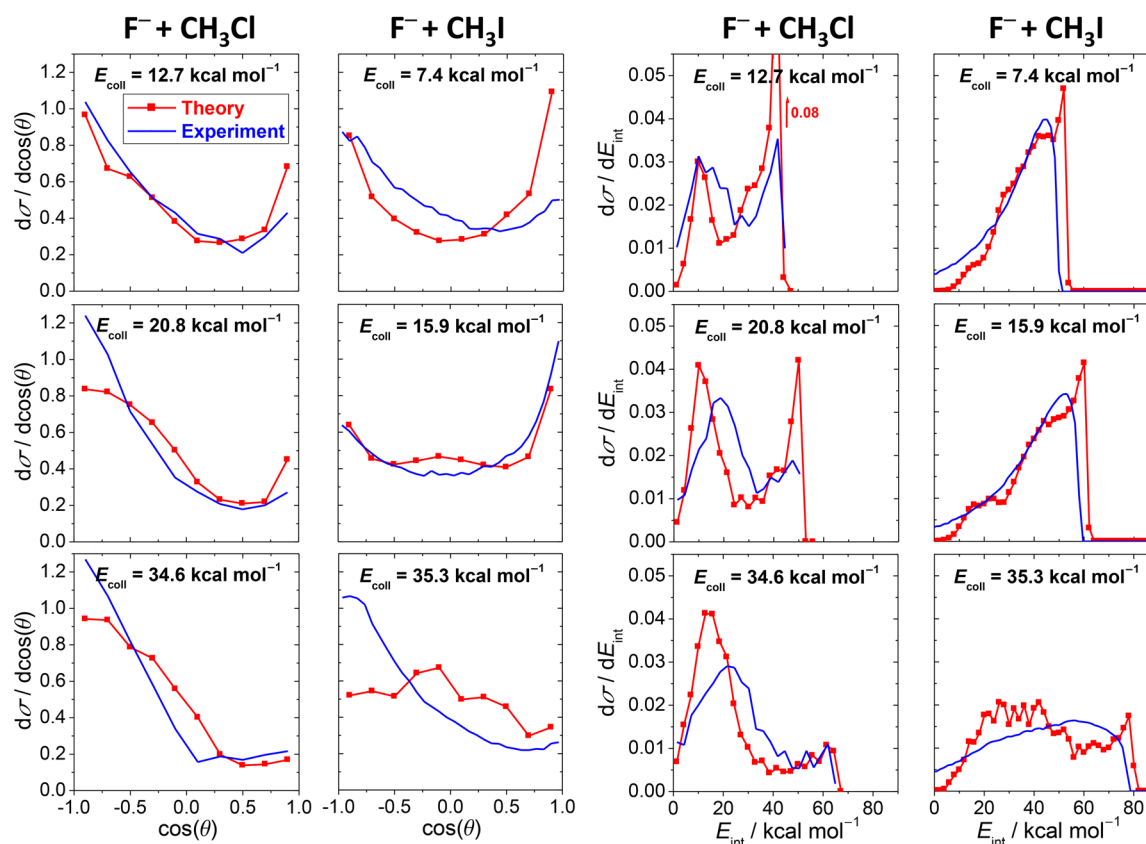


Figure 17. Comparison of the computed and measured normalized scattering angle and product internal energy distributions of the $F^- + CH_3Y$ [$Y = Cl$ and I] S_N2 reactions at different collision energies. The experimental data are taken from refs 49 and 13; the QCT results are taken from refs 49 and 19.

between experimental distributions and the present QCT results support our confidence that the analytical PES-based approach of S_N2 reaction dynamics is a promising research direction.

IV. SUMMARY AND CONCLUSIONS

The history of S_N2 reactions began more than 100 years ago.²¹ Our S_N2 story started only approximately five years ago when we introduced an analytic ab initio PES-based approach to study the dynamics of S_N2 reactions. Whereas traditional direct dynamics computations require millions or billions of gradients, our PESs are fit to only a few tens of thousands of energy points, thereby allowing the use of high-level ab initio theory, while the analytic representation allows the efficient computation of millions of trajectories resulting in unprecedented statistical accuracy for S_N2 reactions. We developed global ab initio PESs for the $F^- + CH_3Y$ [$Y = F, Cl, I$] systems,^{17–19} which describe the S_N2 reactions via the backside attack Walden-inversion and frontside attack pathways as well as the proton-transfer channels leading to $HF + CH_2Y^-$. Moreover, our trajectory simulations revealed a new double-inversion retention pathway, in which a proton-abstraction induced inversion is followed by a second inversion via the usual Walden-TS.¹⁷ Later we identified double-inversion TSs for the $X^- + CH_3Y$ [$X, Y = F, Cl, Br, I$] reactions and concluded that double inversion may be a general retention mechanism for S_N2 reactions.⁵¹ These findings motivated active research, which led to the discovery of double inversion in aqueous solution⁶³ as well as in direct dynamics simulations.⁵³ Double inversion and frontside attack are usually minor S_N2 channels; thus, for their

quantitative description the analytic PESs are essential, because these PESs can provide the millions of trajectories needed for reasonable statistical accuracy. Besides the description of the above-mentioned retention mechanisms, the new analytical PESs made computations possible that have never or rarely been done for S_N2 reactions such as (a) vibrational-mode specific dynamics,^{20,56} (b) rotational-mode specific, that is, JK -dependent, dynamics,⁷³ (c) computations of mode-specific polyatomic product vibrational distributions,^{16,56} (d) determinations of statistically accurate differential cross sections,^{49,18,19} (e) deciphering frontside complex formation via dynamics mapping,⁵⁰ and (f) high-dimensional quantum wave-packet dynamics.²⁰ These computations found that (a) reactant vibrational excitations, especially C–Cl stretching excitation, enhance the $F^- + CH_3Cl$ S_N2 reactions, though significant collision energy dependence and in some cases inhibition were seen, (b) rotational excitations usually decrease S_N2 reactivity with intriguing JK dependence, (c) pure spectator mode picture is not maintained in the $F^- + CHD_2Cl$ S_N2 reaction, (d) scattering angle distributions are usually in excellent agreement with experiment, (e) frontside complex formation is significant in $F^- + CH_3I$, whereas negligible in $F^- + CH_3Cl$, and (f) QCT and quantum results are in good agreement.

We have described results on the reactions of F^- with methyl halides in the gas phase. There are several directions to move forward, for example, (a) studying nucleophile effects by replacing F^- with Cl^- or Br^- or with a more complex ion such as OH^- , CN^- , NH_2^- , etc., (b) replacing methyl halides with larger alkyl halides, such as ethyl halides, (c) adding water molecules to the system thereby studying the solvation effects,

and (d) replacing the carbon center with silicon or nitrogen. We have done or have been doing research toward all of these directions. We already published high-level benchmark characterizations of the complex potential energy surfaces of the $\text{Cl}^- + \text{CH}_3\text{I}$ (ref 48) and $\text{F}^- + \text{CH}_3\text{CH}_2\text{Cl}$ (ref 65) reactions. For the latter the analytic PES development is underway, which will allow studying the competing dynamics of the $\text{S}_{\text{N}}2$ and bimolecular elimination (E2) channels. We believe that the ab initio analytical PES-based approach will be found a powerful tool for uncovering the dynamics and mechanisms of the above-described ion–molecule reactions, by quasi-classical, quantum, and joint experimental–theoretical investigations.

AUTHOR INFORMATION

Corresponding Author

*E-mail: gczako@chem.u-szeged.hu.

ORCID

István Szabó: 0000-0002-3700-3614

Gábor Czako: 0000-0001-5136-4777

Present Address

^aDepartment of Chemistry, King's College London, London SE1 1DB, United Kingdom.

Notes

The authors declare no competing financial interest.

Biographies



István Szabó obtained his Ph.D. in theoretical and physical chemistry at Eötvös University, Budapest, Hungary, in 2016. From September 2015 to July 2016 he was a research assistant at the University of Szeged, Hungary, as a member of the research group of Gábor Czako. Subsequently, he joined Edina Rosta's research group at King's College London, United Kingdom, as an EPSRC postdoctoral research fellow. His current research interests focus on molecular spectroscopy, ab initio potential energy surface developments, reaction dynamics simulations, QM/MM methods, biological electron transfer reactions, and development of Markov model-based analysis and enhanced sampling methods for biomolecular processes. He is also interested in computational design of drugs and nano constructs, as well as in binding properties of supramolecular systems in strong collaboration with the Cavendish Laboratory and Melville Laboratory of Polymer Synthesis at the University of Cambridge, UK.



Gábor Czako received his Ph.D. in theoretical molecular spectroscopy at Eötvös University, Budapest, Hungary, in 2007. From January 2008 he spent nearly four years as a postdoctoral fellow at Emory University, Atlanta, GA, USA, and started to work on the field of chemical reaction dynamics. In December 2011 he returned to Hungary and became a research associate at the Institute of Chemistry, Eötvös University. In 2015 he was invited to join the faculty of the Department of Physical Chemistry and Materials Science, University of Szeged, where he is currently an assistant professor and the head of the Computational Reaction Dynamics Research Group. His current research interests involve potential energy surface developments, reaction dynamics computations, and high-accuracy ab initio thermochemistry. In 2012 he received the Junior Polanyi Prize of the Hungarian Academy of Sciences and the prestigious Junior Prima Prize, given to the most outstanding Hungarian scientists under age 33. In 2017 he obtained the Doctor of the Hungarian Academy of Sciences title, the D.Sc. degree in Hungary, and became the youngest doctor of the Section of Chemical Sciences. His publication record includes papers in Science, PNAS, Nature Chemistry, and Nature Communications.

ACKNOWLEDGMENTS

G.C. thanks the Scientific Research Fund of Hungary (PD-111900 and K-125317) and the János Bolyai Research Scholarship of the Hungarian Academy of Sciences for financial support. We acknowledge the National Information Infrastructure Development Institute for awarding us access to resource based in Hungary at Debrecen and Szeged, where some of the computations were performed. We thank the present and former students of our group, B. Olsz, V. Tajti, T. Györi, G. Kovács, Z. Fábrián, B. Hajdu, G. Szekeres, D. Tasi, and H. Telekes, for their ongoing and/or previous work on $\text{S}_{\text{N}}2$ reactions and the groups of Profs. R. Wester, M. Yang, and H. Guo for the fruitful collaborations.

REFERENCES

- (1) Born, M.; Oppenheimer, R. Zur Quantentheorie der Molekeln. *Ann. Phys.* **1927**, *389*, 457–484.
- (2) Hehre, W. J.; Radom, L.; Schleyer, P. v. R.; Pople, J. A. *Molecular Orbital Theory*; Wiley: New York, 1986.
- (3) Møller, C.; Plesset, M. S. Note on an Approximation Treatment for Many-Electron Systems. *Phys. Rev.* **1934**, *46*, 618–622.
- (4) Čížek, J. On the Correlation Problem in Atomic and Molecular Systems. Calculation of Wavefunction Components in Ursell-Type Expansion Using Quantum-Field Theoretical Methods. *J. Chem. Phys.* **1966**, *45*, 4256–4266.
- (5) Kohn, W.; Sham, L. J. Self-Consistent Equations Including Exchange and Correlation Effects. *Phys. Rev.* **1965**, *140*, A1133–A1138.

- (6) Czakó, G.; Shepler, B. C.; Braams, B. J.; Bowman, J. M. Accurate ab Initio Potential Energy Surface, Dynamics, and Thermochemistry of the $F + CH_4 \rightarrow HF + CH_3$ Reaction. *J. Chem. Phys.* **2009**, *130*, 084301.
- (7) Czakó, G.; Bowman, J. M. Dynamics of the Reaction of Methane with Chlorine Atom on an Accurate Potential Energy Surface. *Science* **2011**, *334*, 343–346.
- (8) Czakó, G.; Bowman, J. M. Dynamics of the $O(^3P) + CHD_3(v_{CH} = 0, 1)$ Reactions on an Accurate ab Initio Potential Energy Surface. *Proc. Natl. Acad. Sci. U. S. A.* **2012**, *109*, 7997–8001.
- (9) Czakó, G. Accurate ab Initio Potential Energy Surface, Thermochemistry, and Dynamics of the $Br(^2P, ^2P_{3/2}) + CH_4 \rightarrow HBr + CH_3$ Reaction. *J. Chem. Phys.* **2013**, *138*, 134301.
- (10) Czakó, G.; Bowman, J. M. Reaction Dynamics of Methane with F, O, Cl, and Br on ab Initio Potential Energy Surfaces. *J. Phys. Chem. A* **2014**, *118*, 2839–2864.
- (11) Sun, L.; Song, K.; Hase, W. L. A S_N2 Reaction That Avoids Its Deep Potential Energy Minimum. *Science* **2002**, *296*, 875–878.
- (12) Zhang, J.; Mikosch, J.; Trippel, S.; Otto, R.; Weidemüller, M.; Wester, R.; Hase, W. L. $F^- + CH_3I \rightarrow FCH_3 + I^-$ Reaction Dynamics. Nontraditional Atomistic Mechanisms and Formation of a Hydrogen-Bonded Complex. *J. Phys. Chem. Lett.* **2010**, *1*, 2747–2752.
- (13) Mikosch, J.; Zhang, J.; Trippel, S.; Eichhorn, C.; Otto, R.; Sun, R.; de Jong, W. A.; Weidemüller, M.; Hase, W. L.; Wester, R. Indirect Dynamics in a Highly Exoergic Substitution Reaction. *J. Am. Chem. Soc.* **2013**, *135*, 4250–4259.
- (14) Manikandan, P.; Zhang, J.; Hase, W. L. Chemical Dynamics Simulations of $X^- + CH_3Y \rightarrow XCH_3 + Y^-$ Gas-Phase S_N2 Nucleophilic Substitution Reactions. Nonstatistical Dynamics and Nontraditional Reaction Mechanisms. *J. Phys. Chem. A* **2012**, *116*, 3061–3080.
- (15) Tachikawa, H.; Igarashi, M. A Direct ab-Initio Dynamics Study on a Gas Phase S_N2 Reaction $F^- + CH_3Cl \rightarrow CH_3F + Cl^-$: Dynamics of Near-Collinear Collision. *Chem. Phys. Lett.* **1999**, *303*, 81–86.
- (16) Szabó, I.; Császár, A. G.; Czakó, G. Dynamics of the $F^- + CH_3Cl \rightarrow Cl^- + CH_3F$ S_N2 Reaction on a Chemically Accurate Potential Energy Surface. *Chem. Sci.* **2013**, *4*, 4362–4370.
- (17) Szabó, I.; Czakó, G. Revealing a Double-Inversion Mechanism for the $F^- + CH_3Cl$ S_N2 Reaction. *Nat. Commun.* **2015**, *6*, 5972.
- (18) Szabó, I.; Telekes, H.; Czakó, G. Accurate ab Initio Potential Energy Surface, Thermochemistry, and Dynamics of the $F^- + CH_3F$ S_N2 and Proton-Abstraction Reactions. *J. Chem. Phys.* **2015**, *142*, 244301.
- (19) Olasz, B.; Szabó, I.; Czakó, G. High-Level ab Initio Potential Energy Surface and Dynamics of the $F^- + CH_3I$ S_N2 and Proton-Transfer Reactions. *Chem. Sci.* **2017**, *8*, 3164–3170.
- (20) Wang, Y.; Song, H.; Szabó, I.; Czakó, G.; Guo, H.; Yang, M. Mode-Specific S_N2 Reaction Dynamics. *J. Phys. Chem. Lett.* **2016**, *7*, 3322–3327.
- (21) Walden, P. Ueber die Gegenseitige Umwandlung Optischer Antipoden. *Ber. Dtsch. Chem. Ges.* **1896**, *29*, 133–138.
- (22) Ingold, C. K. *Structure and Mechanisms in Organic Chemistry*; Cornell University Press: Ithaca, NY, 1953.
- (23) Glukhovtsev, M. N.; Pross, A.; Radom, L. Gas-Phase Identity S_N2 Reactions of Halide Anions with Methyl Halides: A High-Level Computational Study. *J. Am. Chem. Soc.* **1995**, *117*, 2024–2032.
- (24) Glukhovtsev, M. N.; Pross, A.; Radom, L. Gas-Phase Non-Identity S_N2 Reactions of Halide Anions with Methyl Halides: A High-Level Computational Study. *J. Am. Chem. Soc.* **1996**, *118*, 6273–6284.
- (25) Parthiban, S.; de Oliveira, G.; Martin, J. M. L. Benchmark ab Initio Energy Profiles for the Gas-Phase S_N2 Reactions $Y^- + CH_3X \rightarrow CH_3Y + X^-$ ($X, Y = F, Cl, Br$). Validation of Hybrid DFT Methods. *J. Phys. Chem. A* **2001**, *105*, 895–904.
- (26) Gonzales, J. M.; Cox, R. S.; Brown, S. T.; Allen, W. D.; Schaefer, H. F. Assessment of Density Functional Theory for Model S_N2 Reactions: $CH_3X + F^-$ ($X = F, Cl, CN, OH, SH, NH_2, PH_2$). *J. Phys. Chem. A* **2001**, *105*, 11327–11346.
- (27) Gonzales, J. M.; Pak, C.; Cox, R. S.; Allen, W. D.; Schaefer, H. F., III; Császár, A. G.; Tarczay, G. Definitive ab Initio Studies of Model S_N2 Reactions $CH_3X + F^-$ ($X = F, Cl, CN, OH, SH, NH_2, PH_2$). *Chem. - Eur. J.* **2003**, *9*, 2173–2192.
- (28) Glukhovtsev, M. N.; Pross, A.; Schlegel, H. B.; Bach, R. D.; Radom, L. Gas-Phase Identity S_N2 Reactions of Halide Anions and Methyl Halides with Retention of Configuration. *J. Am. Chem. Soc.* **1996**, *118*, 11258–11264.
- (29) Bento, A. P.; Bickelhaupt, F. M. Nucleophilicity and Leaving-Group Ability in Frontside and Backside S_N2 Reactions. *J. Org. Chem.* **2008**, *73*, 7290–7299.
- (30) Zhang, J.; Lourderaj, U.; Addepalli, S. V.; de Jong, W. A.; Hase, W. L. Quantum Chemical Calculations of the $Cl^- + CH_3I \rightarrow CH_3Cl + I^-$ Potential Energy Surface. *J. Phys. Chem. A* **2009**, *113*, 1976–1984.
- (31) Mikosch, J.; Trippel, S.; Eichhorn, C.; Otto, R.; Lourderaj, U.; Zhang, J.-X.; Hase, W. L.; Weidemüller, M.; Wester, R. Imaging Nucleophilic Substitution Dynamics. *Science* **2008**, *319*, 183–186.
- (32) Xie, J.; Otto, R.; Mikosch, J.; Zhang, J.; Wester, R.; Hase, W. L. Identification of Atomic-Level Mechanisms for Gas-Phase $X^- + CH_3Y$ S_N2 Reactions by Combined Experiments and Simulations. *Acc. Chem. Res.* **2014**, *47*, 2960–2969.
- (33) Wester, R. Velocity Map Imaging of Ion–Molecule Reactions. *Phys. Chem. Chem. Phys.* **2014**, *16*, 396–405.
- (34) Xie, J.; Hase, W. L. Rethinking the S_N2 Reaction. *Science* **2016**, *352*, 32–33.
- (35) Meyer, J.; Wester, R. Ion–Molecule Reaction Dynamics. *Annu. Rev. Phys. Chem.* **2017**, *68*, 333–353.
- (36) Czakó, G.; Szabó, I.; Telekes, H. On the Choice of the ab Initio Level of Theory for Potential Energy Surface Developments. *J. Phys. Chem. A* **2014**, *118*, 646–654.
- (37) Raghavachari, K.; Trucks, G. W.; Pople, J. A.; Head-Gordon, M. A Fifth-Order Perturbation Comparison of Electron Correlation Theories. *Chem. Phys. Lett.* **1989**, *157*, 479–483.
- (38) Werner, H.-J.; Adler, T. B.; Manby, F. R. General Orbital Invariant MP2-F12 Theory. *J. Chem. Phys.* **2007**, *126*, 164102.
- (39) Adler, T. B.; Knizia, G.; Werner, H.-J. A Simple and Efficient CCSD(T)-F12 Approximation. *J. Chem. Phys.* **2007**, *127*, 221106.
- (40) Dunning, T. H., Jr. Gaussian Basis Sets for Use in Correlated Molecular Calculations. I. The Atoms Boron Through Neon and Hydrogen. *J. Chem. Phys.* **1989**, *90*, 1007–1023.
- (41) Peterson, K. A.; Dunning, T. H., Jr. Accurate Correlation Consistent Basis Sets for Molecular Core–Valence Correlation Effects: The Second Row Atoms Al–Ar, and the First Row Atoms B–Ne Revisited. *J. Chem. Phys.* **2002**, *117*, 10548–10560.
- (42) Peterson, K. A.; Figgen, D.; Goll, E.; Stoll, H.; Dolg, M. Systematically Convergent Basis Sets with Relativistic Pseudopotentials. II. Small-Core Pseudopotentials and Correlation Consistent Basis Sets for the Post- d Group 16–18 Elements. *J. Chem. Phys.* **2003**, *119*, 11113–11123.
- (43) Braams, B. J.; Bowman, J. M. Permutationally Invariant Potential Energy Surfaces in High Dimensionality. *Int. Rev. Phys. Chem.* **2009**, *28*, 577–606.
- (44) Bowman, J. M.; Czakó, G.; Fu, B. High-Dimensional ab Initio Potential Energy Surfaces for Reaction Dynamics Calculations. *Phys. Chem. Chem. Phys.* **2011**, *13*, 8094–8111.
- (45) Allen, W. D.; East, A. L. L.; Császár, A. G. In *Structures and Conformations of Non-Rigid Molecules*; Laane, J., Dakkouri, M., van der Veken, B., Oberhammer, H., Eds.; Kluwer: Dordrecht, The Netherlands, 1993; p 343.
- (46) Császár, A. G.; Allen, W. D.; Schaefer, H. F. Pursuit of the ab Initio Limit for Conformational Energy Prototypes. *J. Chem. Phys.* **1998**, *108*, 9751–9764.
- (47) Xie, J.; Zhang, J.; Hase, W. L. Is There Hydrogen Bonding for Gas Phase S_N2 Pre-Reaction Complexes? *Int. J. Mass Spectrom.* **2015**, *378*, 14–19.
- (48) Szabó, I.; Czakó, G. Benchmark ab Initio Characterization of the Complex Potential Energy Surface of the $Cl^- + CH_3I$ Reaction. *J. Phys. Chem. A* **2017**, *121*, 5748–5757.
- (49) Stei, M.; Carrascosa, E.; Kainz, M. A.; Kelkar, A. H.; Meyer, J.; Szabó, I.; Czakó, G.; Wester, R. Influence of the Leaving Group on the Dynamics of a Gas-Phase S_N2 Reaction. *Nat. Chem.* **2016**, *8*, 151–156.

- (50) Szabó, I.; Olasz, B.; Czakó, G. Deciphering Front-Side Complex Formation in S_N2 Reactions via Dynamics Mapping. *J. Phys. Chem. Lett.* **2017**, *8*, 2917–2923.
- (51) Szabó, I.; Czakó, G. Double-Inversion Mechanisms of the $X^- + CH_3Y$ [$X, Y = F, Cl, Br, I$] S_N2 Reactions. *J. Phys. Chem. A* **2015**, *119*, 3134–3140.
- (52) Zhang, J.; Xie, J.; Hase, W. L. Dynamics of the $F^- + CH_3I \rightarrow HF + CH_2I^-$ Proton Transfer Reaction. *J. Phys. Chem. A* **2015**, *119*, 12517–12525.
- (53) Ma, Y.-T.; Ma, X.; Li, A.; Guo, H.; Yang, L.; Zhang, J.; Hase, W. L. Potential Energy Surface Stationary Points and Dynamics of the $F^- + CH_3I$ Double Inversion Mechanism. *Phys. Chem. Chem. Phys.* **2017**, *19*, 20127–20136.
- (54) Czakó, G.; Bowman, J. M. Quasiclassical Trajectory Calculations of Correlated Product Distributions for the $F + CHD_3(v_1 = 0, 1)$ Reactions Using an ab Initio Potential Energy Surface. *J. Chem. Phys.* **2009**, *131*, 244302.
- (55) Czakó, G. Gaussian Binning of the Vibrational Distributions for the $Cl + CH_4(v_{4/2} = 0, 1) \rightarrow H + CH_3Cl(n_1n_2n_3n_4n_5n_6)$ Reactions. *J. Phys. Chem. A* **2012**, *116*, 7467–7473.
- (56) Szabó, I.; Czakó, G. Mode-Specific Multi-Channel Dynamics of the $F^- + CHD_2Cl$ Reaction on a Global ab Initio Potential Energy Surface. *J. Chem. Phys.* **2016**, *145*, 134303.
- (57) Sierra, J. D.; Bonnet, L.; González, M. Quasi-Classical Trajectory–Gaussian Binning Study of the $OH + D_2 \rightarrow HOD-(v_1', v_2', v_3')$ + D Angle–Velocity and Vibrational Distributions at a Collision Energy of 0.28 eV. *J. Phys. Chem. A* **2011**, *115*, 7413–7417.
- (58) Bonnet, L.; Espinosa-García, J.; Corchado, J. C.; Liu, S.; Zhang, D. H. Classical Versus Quantum Vibrational State Distributions for the Benchmark Polyatomic Reaction $OH + D_2$: Checking the Validity of the QCT Method. *Chem. Phys. Lett.* **2011**, *516*, 137–140.
- (59) García, E.; Corchado, J. C.; Espinosa-García, J. A Detailed Product Distribution Analysis of Some Potential Energy Surfaces Describing the $OH + CO \rightarrow H + CO_2$ Reaction. *Comput. Theor. Chem.* **2012**, *990*, 47–52.
- (60) Bonnet, L.; Espinosa-García, J. Simulation of the Experimental Imaging Results for the $OH + CHD_3$ Reaction with a Simple and Accurate Theoretical Approach. *Phys. Chem. Chem. Phys.* **2017**, *19*, 20267–20270.
- (61) Czakó, G.; Wang, Y.; Bowman, J. M. Communication: Quasiclassical Trajectory Calculations of Correlated Product-State Distributions for the Dissociation of $(H_2O)_2$ and $(D_2O)_2$. *J. Chem. Phys.* **2011**, *135*, 151102.
- (62) Ch'ng, L. C.; Samanta, A. K.; Czakó, G.; Bowman, J. M.; Reisler, H. Experimental and Theoretical Investigations of Energy Transfer and Hydrogen-Bond Breaking in the Water Dimer. *J. Am. Chem. Soc.* **2012**, *134*, 15430–15435.
- (63) Liu, P.; Wang, D. Y.; Xu, Y. A New, Double-Inversion Mechanism of the $F^- + CH_3Cl$ S_N2 Reaction in Aqueous Solution. *Phys. Chem. Chem. Phys.* **2016**, *18*, 31895–31903.
- (64) Liu, P.; Zhang, J.; Wang, D. Y. Multi-Level Quantum Mechanics Theories and Molecular Mechanics Study of the Double-Inversion Mechanism of the $F^- + CH_3I$ Reaction in Aqueous Solution. *Phys. Chem. Chem. Phys.* **2017**, *19*, 14358–14365.
- (65) Tajti, V.; Czakó, G. Benchmark ab Initio Characterization of the Complex Potential Energy Surface of the $F^- + CH_3CH_2Cl$ Reaction. *J. Phys. Chem. A* **2017**, *121*, 2847–2854.
- (66) Song, H.; Guo, H. Vibrational and Rotational Mode Specificity in the $Cl + H_2O \rightarrow HCl + OH$ Reaction: A Quantum Dynamical Study. *J. Phys. Chem. A* **2015**, *119*, 6188–6194.
- (67) Song, H.; Lee, S.-Y.; Lu, Y.; Guo, H. Full-Dimensional Quantum Dynamical Studies of the $Cl + HOD \rightarrow HCl/DCl + OD/OH$ Reaction: Bond Selectivity and Isotopic Branching Ratio. *J. Phys. Chem. A* **2015**, *119*, 12224–12230.
- (68) Czakó, G.; Liu, R.; Yang, M.; Bowman, J. M.; Guo, H. Quasiclassical Trajectory Studies of the $O(^3P) + CX_4(v_k = 0, 1) \rightarrow OX(v) + CX_3(n_1n_2n_3n_4)$ [$X = H$ and D] Reactions on an ab Initio Potential Energy Surface. *J. Phys. Chem. A* **2013**, *117*, 6409–6420.
- (69) Xie, C.; Jiang, B.; Yang, M.; Guo, H. State-to-State Mode Specificity in $F + CHD_3 \rightarrow HF/DF + CD_3/CHD_2$ Reaction. *J. Phys. Chem. A* **2016**, *120*, 6521–6528.
- (70) Riedel, J.; Yan, S.; Liu, K. Mode Specificity in Reactions of Cl with CH_2 Stretch-Excited $CH_2D_2(v_1, v_6 = 1)$. *J. Phys. Chem. A* **2009**, *113*, 14270–14276.
- (71) Hase, W. L. *Encyclopedia of Computational Chemistry*; Wiley: New York, 1998, pp 399–407.
- (72) Liu, R.; Wang, F.; Jiang, B.; Czakó, G.; Yang, M.; Liu, K.; Guo, H. Rotational Mode Specificity in the $Cl + CHD_3 \rightarrow HCl + CD_3$ Reaction. *J. Chem. Phys.* **2014**, *141*, 074310.
- (73) Szabó, I.; Czakó, G. Rotational Mode Specificity in the $F^- + CH_3Y$ [$Y = F$ and Cl] S_N2 reactions. *J. Phys. Chem. A* **2015**, *119*, 12231–12237.
- (74) Zhang, D. H.; Light, J. C. Quantum State-to-State Reaction Probabilities for the $H + H_2O \rightarrow H_2 + OH$ Reaction in Six Dimensions. *J. Chem. Phys.* **1996**, *105*, 1291–1294.
- (75) Li, J.; Jiang, B.; Song, H.; Ma, J.; Zhao, S.; Dawes, R.; Guo, H. From ab Initio Potential Energy Surfaces to State-Resolved Reactivities: $X + H_2O \leftrightarrow HX + OH$ [$X = F, Cl, \text{ and } O(^3P)$] Reactions. *J. Phys. Chem. A* **2015**, *119*, 4667–4687.
- (76) Yang, M.; Lee, S.-Y.; Zhang, D. H. Seven-Dimensional Quantum Dynamics Study of the $O(^3P) + CH_4$ Reaction. *J. Chem. Phys.* **2007**, *126*, 064303.
- (77) Yang, M.; Zhang, D. H.; Lee, S.-Y. A Seven-Dimensional Quantum Study of the $H + CH_4$ Reaction. *J. Chem. Phys.* **2002**, *117*, 9539–9542.
- (78) Zhang, Z.; Zhou, Y.; Zhang, D. H.; Czakó, G.; Bowman, J. M. Theoretical Study of the Validity of the Polanyi Rules for the Late-Barrier $Cl + CHD_3$ Reaction. *J. Phys. Chem. Lett.* **2012**, *3*, 3416–3419.
- (79) Welsch, R.; Manthe, U. Full-Dimensional and Reduced-Dimensional Calculations of Initial State-Selected Reaction Probabilities Studying the $H + CH_4 \rightarrow H_2 + CH_3$ Reaction on a Neural Network PES. *J. Chem. Phys.* **2015**, *142*, 064309.
- (80) Qi, J.; Song, H.; Yang, M.; Palma, J.; Manthe, U.; Guo, H. Communication: Mode Specific Quantum Dynamics of the $F + CHD_3 \rightarrow HF + CD_3$ Reaction. *J. Chem. Phys.* **2016**, *144*, 171101.
- (81) Clary, D. C.; Palma, J. Quantum Dynamics of the Walden Inversion Reaction $Cl^- + CH_3Cl \rightarrow ClCH_3 + Cl^-$. *J. Chem. Phys.* **1997**, *106*, 575–583.
- (82) Yu, H.-G.; Nyman, G. An Application of the Rotating Line Umbrella Model to Quantum Dynamics of S_N2 Reactions. *Chem. Phys. Lett.* **1999**, *312*, 585–590.
- (83) Hennig, C.; Schmatz, S. State-Selected Dynamics of the Complex-Forming Bimolecular Reaction $Cl^- + CH_3Cl' \rightarrow ClCH_3 + Cl^-$: A Four-Dimensional Quantum Scattering Study. *J. Chem. Phys.* **2004**, *121*, 220–236.
- (84) Hennig, C.; Schmatz, S. Four-Dimensional Quantum Study on Exothermic Complex-Forming Reactions: $Cl^- + CH_3Br \rightarrow ClCH_3 + Br^-$. *J. Chem. Phys.* **2005**, *122*, 234307.
- (85) Hennig, C.; Schmatz, S. Differential Reaction Cross Sections from Rotationally Resolved Quantum Scattering Calculations: Application to Gas-Phase S_N2 Reactions. *Phys. Chem. Chem. Phys.* **2012**, *14*, 12982–12991.
- (86) Li, Y.; Wang, Y.; Wang, D. Y. Quantum Dynamics Study of the Potential Energy Minima Effect on Energy Efficiency for the $F^- + CH_3Cl \rightarrow FCH_3 + Cl^-$ Reaction. *J. Phys. Chem. A* **2017**, *121*, 2773–2779.